ORIGINAL ARTICLE

CrossMark

Dentin sealing and antibacterial effects of silver-doped bioactive glass/mesoporous silica nanocomposite: an in vitro study

Jae-Hyun Jung[1] · Dong-Hyun Kim[2] · Kyung-Hyeon Yoo[3] · Seog-Young Yoon[3] · Yeon Kim[4] · Moon-Kyoung Bae[4] · Jin Chung[5] · Ching-Chang Ko[6] · Yong Hoon Kwon[7] · Yong-Il Kim[1,8]

Abstract

Objectives To synthesize a silver-doped bioactive glass/mesoporous silica nanoparticle (Ag-BGN@MSN), as well as to investigate its effects on dentinal tubule occlusion, microtensile bond strength (MTBS), and antibacterial activity.

Materials and methods Ag-BGN@MSN was synthesized using a modified "quick alkali-mediated sol-gel" method. Demineralized tooth disc models were made and divided into four groups; the following treatments were then applied: group 1—no treatment, group 2—bioglass, group 3—MSN, group 4—Ag-BGN@MSN. Next, four discs were selected from each group and soaked into 6 wt% citric acid to test acid-resistant stability. Dentinal tubule occlusion, as well as the occlusion ratio, was observed using field-emission scanning electron microscopy. The MTBS was also measured to evaluate the desensitizing effect of the treatments. Cytotoxicity was examined using the MTT assay. Antibacterial activity was detected against *Lactobacillus casei*, and ion dissolution was evaluated using inductively coupled plasma optical emission spectrometry.

Results Ag-BGN@MSN effectively occluded the dentinal tubule and formed a membrane-like layer. After the acid challenge, Ag-BGN@MSN had the highest rate of dentinal tubule occlusion. There were no significant differences in MTBS among the four groups ($P > 0.05$). All concentrations of Ag-BGN@MSN used had a relative cell viability above 72%.

Yong Hoon Kwon and Yong-Il Kim contributed equally to this article.

✉ Yong Hoon Kwon
y0k0916@pusan.ac.kr

✉ Yong-Il Kim
kimyongil@pusan.ac.kr

Jae-Hyun Jung
hyunny140@hanmail.net

Dong-Hyun Kim
kimnano75@pusan.ac.kr

Kyung-Hyeon Yoo
seweet07@pusan.ac.kr

Seog-Young Yoon
syy3@pusan.ac.kr

Yeon Kim
graceyeon88@gmail.com

Moon-Kyoung Bae
mkbae@pusan.ac.kr

Jin Chung
jchung@pusan.ac.kr

Ching-Chang Ko
ching_ChangKo@unc.edu

[1] Department of Orthodontics, Dental Research Institute, Pusan National University Dental Hospital, Geumoro 20, Mulgeum, Yangsan 50612, Republic of Korea

[2] R&D Center, Upex. Med Co., Ltd., Hagui-ro 282, Dongan-gu, Anyang, Gyeonggi-do 14056, Republic of Korea

[3] School of Materials Science and Engineering, Pusan National University, Busandaehak-ro 63beon-gil, Geumjeong-gu, Busan 46241, Republic of Korea

[4] Department of Oral Physiology, School of Dentistry, Pusan National University, Busandaehak-ro 49, Mulgeum, Yangsan 50612, Republic of Korea

[5] Department of Oral Microbiology, School of Dentistry, Pusan National University, Busandaehak-ro 49, Mulgeum, Yangsan 50612, Republic of Korea

[6] Department of Orthodontics, School of Dentistry, University of North Carolina at Chapel Hill, Chapel Hill, NC 27516, USA

[7] Department of Dental Materials, Pusan National University, Busandaehak-ro 49, Mulgeum, Yangsan 50612, Republic of Korea

[8] Institute of Translational Dental Sciences, School of Dentistry, Pusan National University, Busandaehak-ro 49, Mulgeum, Yangsan 50612, Republic of Korea

🌀 Springer

Conclusions Ag-BGN@MSN was successfully fabricated using a modified sol-gel method. The Ag-BGN@MSN biocomposite effectively occluded dentinal with acid-resistant stability, did not decrease bond strength in self-etch adhesive system, had low cytotoxicity, and antibacterial effect.

Clininal relevance Dentinal tubule sealing induced by Ag-BGN@MSN biocomposite with antibacterial effect is likely to increase long-term stability in DH.

Keywords Bioactive glass · Mesoporous silica · Nanoparticle · Antibacterial effect · Remineralization · Dentin hypersensitivity

Introduction

Dentin hypersensitivity (DH) is a common problem encountered by dentists in clinics. The condition is characterized by dentin exposure and is accompanied by sudden and sharp pain and discomfort in the presence of heat, steam, contact, osmotic pressure, or chemical stimulation. The cause of this dentin exposure is loss of enamel due to abrasion, attrition, or acid erosion; gingival recession caused by gingivitis or periodontal surgery may also play a role [1–3]. The reported incidence rate of DH ranges from 4 to 74%; the reason for this broad variation is differences in research methods and subjects [4–8]. With regard to the mechanism of DH, the literature has presented a number of theories—namely the "direct innervations," "odontoblast receptor," and "hydrodynamic" theories. Recently, the hydrodynamic theory in particular has become widely accepted [9].

Clinicians have taken various approaches to DH treatment: (1) nerve desensitization, (2) protein precipitation, (3) dentinal tubule plugging, (4) dentin adhesive sealing, (5) dentin bonding agents, and (6) various laser treatments [1]. Some of these treatment methods have successfully occluded the dentinal tubules and blocked fluid flow, thus reducing clinical symptoms. However, these methods are limited in that their depth of penetration is limited to the dental surface. For this reason, exposure to dietary acid re-exposes the dentinal tubules, resulting in a short-lasting treatment effect and relapse of hypersensitivity [10–13].

Thus, effective occlusion of dentinal tubules and long-lasting stability upon exposure to dietary acid is necessary to ensure that DH is effectively treated [14, 15]. Furthermore, in clinical circumstances, since tooth sensitivity is often accompanied by enamel defects, resin-based restoration is frequently required, and clinicians must ensure that DH treatment does not affect the bonding strength of the resins [16].

Mesoporous silica nanoparticles (MSNs) are widely used in the biomedical field because they have a stable structure, large surface area/mass ratio, high adsorbability, and high thermostability and chemostability. Because of the stability and high transportation ability of MSNs, they are often used as the ideal mediator of medicines, genes, and functional nanoparticles [17, 18]. In particular, Tian et al. reported that MSNs coated with Ca^{2+} or PO_4^{3-} can effect dentinal tubule occlusion and remineralization [19].

Similarly, bioactive glasses (BGs) have been used as biomedical materials to encourage osteogenesis because of their osteoconductivity and ion-release capability. Therefore, in vitro research has suggested that BGs can induce remineralization on the dentin disc surfaces [20]. BG nanoparticles (BGNs) have a larger surface area/mass ratio than conventional BGs, as well as greater illumination intensity, hydrophobicity, and wettability. For this reason, BGNs affect cell adhesion and confer bonding properties on host tissue, and they therefore have increased bioactivity [21, 22]. Additional advantages, such as soft tissue regeneration, wound healing, and antibacterial effects, can be obtained when the ions Ag^+, Cu^+, and Sr^{2+} are superinduced during BG synthesis [23, 24]. In particular, silver has broad antibacterial activity, and the addition of Ag^+ ions is the most common approach to synthesizing biomedical materials that have antibacterial capabilities [25]. It follows that silver-doped BGNs (Ag-BGNs) would have all the characteristics of BGNs, as well as an antibacterial effect [26].

By way of comparison of the two substances above, MSNs have a large surface area/mass ratio, but lack bioactivity, while BGNs have a smaller surface area than MSNs, but larger bioactivity [27]. Therefore, dentinal tubule occlusion and sealing using an Ag-BGN-coated MSN (Ag-BGN@MSN) biocomposite material is worthy of study as a treatment option for DH. However, no proper research has yet been carried out on this subject.

Thus, the aim of the present study was to synthesize an Ag-BGN@MSN biocomposite material, as well as to investigate the materials characteristics, including whether it can occlude dentinal tubules effectively, maintain stability in the presence of acid, preserve microtensile bond strength (MTBS), and confer an antibacterial effect.

Materials and method

Synthesis of an Ag-doped BGN-coated MSN

The MSNs (200 nm) were purchased from Sigma-Aldrich (St. Louis, MO, USA), and the Ag-BGN@MSN was synthesized using a modified version the "quick alkali-mediated sol-gel" method described by Xia et al. [28]. Briefly, 2.8 ml of 2 M HNO_3, 13.9 ml of deionized water

(DIW), and 1.0 g of MSNs were added to 50 ml of ethanol. Next, 21.6 ml of tetraethyl orthosilicate was added, and the preparation was vigorously stirred at room temperature. Triethyl phosphate (2.2 ml) was then added, and the preparation was stirred again for 30 min. Subsequently, to prepare 1, 3, and 5% Ag-BGN@MSN, $Ca(NO_3)_2 \cdot 4H_2O$ was added (13.50, 12.76, 11.91, respectively), and the preparation was stirred for another 30 min. Next, $AgNO_3$ was added (0.15, 0.44, and 0.7, respectively), and the preparation was stirred for 1 h, followed by aging for 24 h at 60 °C. After gelation, the preparation was oven dried at 80 °C. The final sample was obtained after calcination for 5 h at 600 °C.

Characteristics of the material

The MSNs and final samples were characterized as follows. X-ray diffraction (XRD) patterns were obtained using an Ultima IV multipurpose XRD system (Rigaku, The woodland, TX, USA) at 40 kV and 40 mA, with a scanning speed of 0.1°/min. Functionalized surfaces were investigated using the ATR method of Fourier transform infrared spectroscopy (FT-IR); specifically, the Spectrum GX FT-IR Spectrometer (PerkinElmer Inc., Waltham, USA) was used. Furthermore, using an adsorption analyzer (autosorb-iQ; Quantachome, Boynton, FL, USA), the N_2 adsorption-desorption isotherms were processed. The distributions of specific surface area and pore size were measured using the Brunauer–Emmett–Teller (BET) and Barrett–Joyner–Halenda (BJH) methods, respectively. The shape of the samples was observed using field-emission scanning electron microscopy (FESEM; SUPRA25; Carl Zeiss, Germany). A 200-kV field-emission transmission electron microscope (FETEM; TALOS F200X; FEI, Hillsboro, OR, USA) was used to observe the samples, and qualitative analysis of the Ag inside the samples was performed using fast analytical energy-dispersive X-ray spectroscopy.

Fabrication of samples and experimental design

This study was reviewed and approved by the Institutional Review Board of 00000 Hospital (PNUDH-2016-033). Thirty-two premolars that had been extracted as part of orthodontic treatment were obtained after informed consent had been given. The teeth were stored in 0.5% thymol solution at 4 °C, and they were used within 3 months. Using a low-speed diamond saw (Struers Accutom-50; Ballerup, Denmark) underwater, a 1-mm thick dentin disc was prepared by slicing the teeth perpendicular to the longitudinal. The disc was polished for 60 s using 320- and 600-grit silicon carbide (SiC) polishing paper. Next, the disc was soaked in 1 wt% citric acid solution for 20 s and rinsed thoroughly by water spray. In this way, the dentinal tubule of the disc was opened to create a demineralized tooth model [17]. The discs were then divided randomly into four groups ($n = 8$ in each): group 1—no treatment (control); group 2—slurry prepared using 100 mg of BG 45S5 (45 SiO-24.5 CaO-24.5 Na_2O-6P_2O; Aladdin Industrial Corporation, Shanghai, China) was applied to the dentin surface using a rotary cup for 30 s under low speed; group 3—slurry prepared using 100 mg of MSNs and 200 μL of DIW was applied using the same method as in group 2; group 4—slurry prepared using 100 mg of Ag-BGN@MSNs and 200 μL of DIW was applied to the dentin surface using the same method as in group 2.

Four discs were randomly selected from each group, and the rest of the discs were prepared for post-treatment. To examine resistance to strong acidic conditions, after applying samples in dentin disc, the discs were soaked in 6 wt% citric acid solution (pH 1.5) for 60 s and rinsed thoroughly using DIW ($n = 4$).

Field-emission scanning electron microscopy assessment of dentin tubule occlusion

The completed samples were stored in a 100% humidified atmosphere at 37 °C for 14 days. To evaluate each disc's treatment and cutting surfaces, the discs were dissected through the longitudinal axis. They were water sprayed and dried to allow sputter-coating with platinum. The change in the exposed dentinal tubule occlusion was then observed using FESEM. The center of each disc was observed using ×2000, ×5000, and ×10,000 microscopic magnification. To calculate the area ratio of the occluded dentinal tubules (area of occluded tubule/the total tubule area), Image J (version 1.50; NIH, Bethesda, MD, USA) was used.

Microtensile bond strength test

To expose the mid-coronal dentin, 20 extra premolars were dissected parallel to the occlusal plane using low-speed diamond saw. The exposed surface was then polished using 600-grit SiC paper and soaked for 20 s in 1 wt% citric acid solution. Subsequently, the tooth models were randomly divided into four groups ($n = 5$ in each). Each group was treated using the methods mentioned in "Microtensile bond strength test"; the samples were then rinsed using water spray for 30 s and air-dried. The following procedure was used to evaluate the effect of the desensitizing treatment on MTBS: Clearfil SE Bond (Kuraray Co., Osaka, Japan) was applied to the dentin surface, according to the manufacturer's instructions. Next, 4-mm height resin composite (Filtek Z 100; 3 M ESPE, St Paul, MN, USA) build-ups were prepared and light-cured for 20 s using an LED curing unit (DEMI; > 1000 mW/cm^2; Kerr Corporation, Middleton, WI, USA).

The samples were stored in 37 °C DIW for 24 h; each sample was then truncated perpendicular to the bonding interface to obtain eight beams with dimensions of 0.9 mm ×

0.9 mm. Each beam was then fixed to the MTBS tester (Bisco; Schaumburg, IL, USA) using cyanoacrylate adhesive, and the tensile force was set for a cross-head speed of 1 mm/min.

Cell culture and cytotoxicity assay

Human dental pulp cells (HDPCs) were separated from the healthy human dental pulp tissue of premolars that had been extracted for orthodontic treatments. The separated pulp tissue was cultivated in an α-modified essential medium (Dulbecco's modified Eagle's medium; LM001-01; Welgene, Seoul, South Korea). Next, 10% fetal bovine serum (Gibco, CA, USA), 100 units/mL penicillin, and 100 mg/mL streptomycin were added to the medium at 37 °C in a 5% CO_2, humidified atmosphere. The medium was replaced every 2 days. The in vitro cytotoxicity of Ag-BGN@MSNs was examined using the 3-(4,5-dimethylthiazol-2-yl)-2,5-diphenyltetrazolium bromide (MTT) assay. Specifically, Ag-BGN@MSN was placed in a 96-well plate (0, 10, 20, 40, 80, 160, and 320 μg/mL density, mixed with DIW), and the DIW was evaporated. Subsequently, 10,000 HDPCs were seeded on each well and cultivated for 24, 48, or 72 h at 37 °C in 5% CO_2. Next, 5 mg/ml of MTT (Sigma-Aldrich, St. Louis, MO, USA) was added to each well; this was followed by 3 h of cultivation. Subsequently, the samples were washed using dimethyl sulfoxide for 5 min, and their optical density was measured at a wavelength of 540 nm. Experiments were triplicated for comparison.

Antibacterial activity test

Next, 200 μl MSN and 1, 3, and 5% Ag-BGN@MSN (0, 200, 300, 400 μg/ml in DIW) was placed in a 96-well plate and the DIW was dried out. *Lactobacillus (L.) casei* (kctc3260) (1.0×10^5 CFU/ml) was then cultured in de Man, Rogosa, and Sharpe (MRS) medium at 37 °C in 5% CO_2 for 24 h. After cultivation, the optical density was measured at a wavelength of 650 nm.

In vitro ion dissolution test

The characteristics of ion dissolution were evaluated using inductively coupled plasma optical emission spectrometry (Optima 8300; PerkinElmer, Waltham, MA, USA). Briefly, 0.5 g of 1, 3, of 5% Ag-BGN@MSN was placed in 5 ml of ×5 stimulated body fluid (Biosesang; Seoul, South Korea), and the density of the ions eluted was measured after 1, 3, 7, 14, 30, and 90 days.

Statistical analysis

To compare among the groups, one-way analysis of variance (ANOVA), with Bonferroni's multiple comparison

tests, was performed. All statistical analyses were conducted using the R language program (version 3.3.2; R Foundation for Statistical Computing, Vienna, Austria).

Results

Characterizations

X-ray diffraction

Figure 1 shows the XRD patterns for the MSN, as well as for the 1, 3, and 5% Ag-BGN@MSN. In the small-angle XRD (Fig. 1a), the MSNs showed peaks at the (100), (110), and (200) planes; this matches with the peak planes of silica. The peaks of the 1, 3, and 5% Ag-BGN@MSN were similar to each other and matched those of silver. Unlike the MSNs, the silver-doped MSNs showed invisible (110) and (200) planes. A similar pattern, with slightly broadened peaks, was observed for the 1, 3, and 5% Ag-BGN@MSN, suggesting that the Ag-BGN@MSN coreshell particles maintain two-dimensional hexagonal structures.

In the wide-angle XRD (Fig. 1b), all samples showed a non-crystalline structure, implying that the material is amorphous.

Fourier transform infrared spectroscopy

To determine the chemical composition of the Ag-BGN@MSN, as well as the chemical stability of MSNs as a core material, the Ag-BGN@MSN was characterized using FT-IR spectroscopy. As shown in Fig. 2a, the silicate adsorption bands of all the core material samples could be observed in all spectra; the peaks at around 1060 and 800 cm^{-1} were ascribed to Si-O-Si.

However, the FT-IR spectrum showed that the decrease in the Si-O-Si peak of Ag-BGN@MSN was associated with shell formation due to the glassy properties of the BG. In the case of pure MSNs (Fig. 2b), the broad bands at approximately 3449 cm^{-1} (data not shown) and 1623 cm^{-1} were ascribed to the presence of Si-O-H vibration. Other typical bands Si-O-Si vibration occurred at around 1243 and 808 cm^{-1}, and Si-OH bending deformation bands can be seen at around 977 cm^{-1}.

The FT-IR spectrum of the 3% Ag-BGN@MSN is presented in Fig. 2c. The spectra of 3% Ag-BGN@MSN revealed vibration bands similar to those of MSN. However, the two sharp bands at 1203 and 1219 cm^{-1} corresponded to silicate adsorption bands representing Si–O–Si stretching of nonbridging oxygen atoms within the silicate tetrahedron. The peak at around 802 cm^{-1} can be attributed to P–O bending in the PO_4^{3-} groups.

Fig. 1 **a** Small-angle X-ray diffraction (XRD) pattern of Ag-BGN@MSN and MSNs. **b** Wide-angle XRD pattern of Ag-BGN@MSN and MSNs
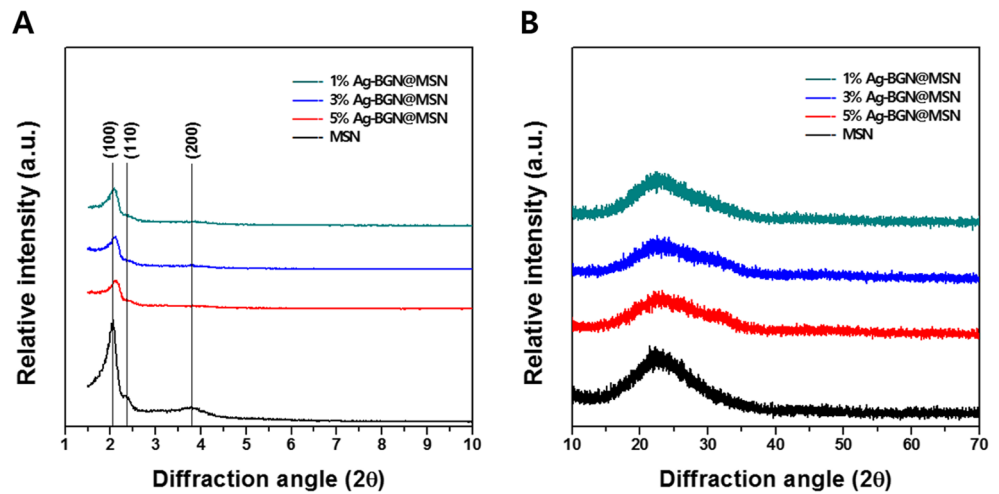
N$_2$ adsorption

N$_2$ adsorption-desorption isotherms were used to assess porosity. Due to the tiny capillary pore structure, the MSNs and Ag-BGN@MSN showed type IV isotherm. Moreover, MSNs had the characteristics of a type-H1 hysteresis loop (Fig. 3), perhaps because they contain uniformly distributed pores. In contrast, Ag-BGN@MSN exhibited the characteristics of a type-H3 hysteresis loop, owing to the aggregation of non-rigid aggregate, or perhaps to the slit-shaped pores of the
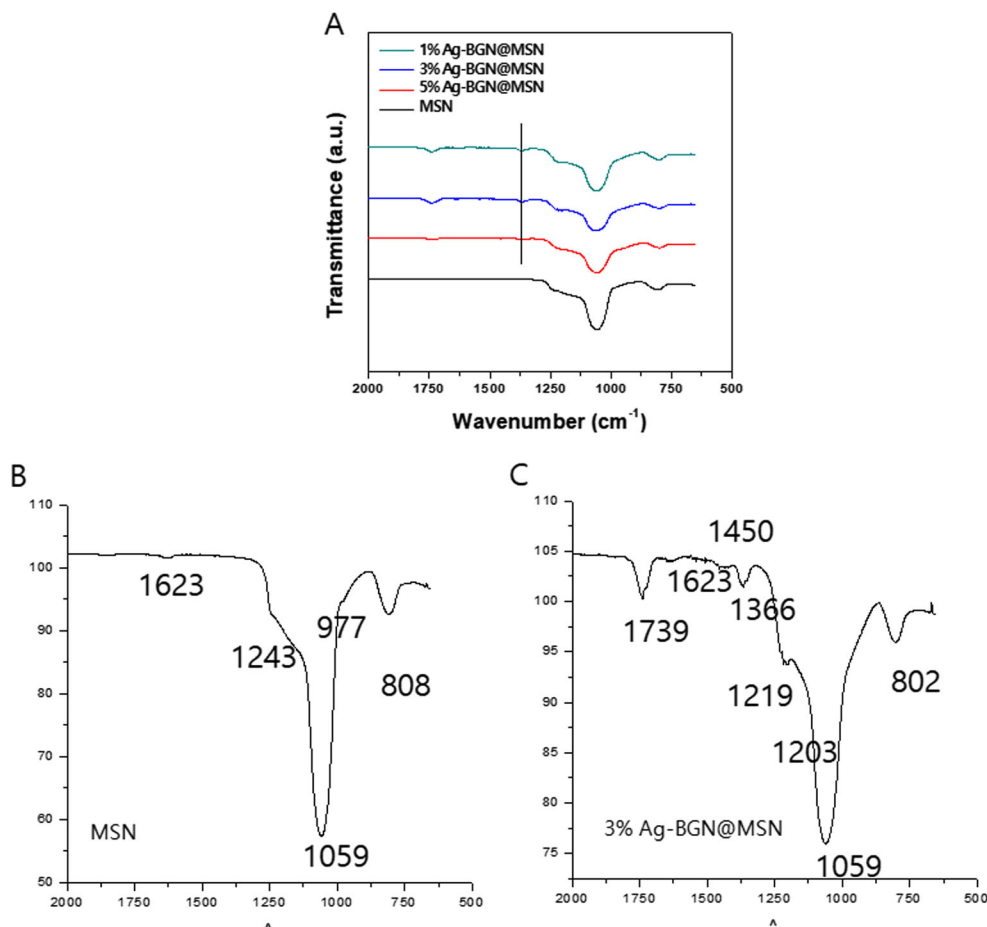

Fig. 2 **a** FT-IR spectra of the Ag-BGN@MSN and MSNs **b** Pure MSNs: typical Si-O-Si vibration bands occur at around 1243 and 808 cm^{-1}, and Si-OH bending deformation bands can be seen at around 977 cm^{-1}. **c** 3% Ag-BGN@MSN reveals vibration bands similar to those of the MSNs: the 1203 and 1219 cm^{-1} bands correspond to silicate adsorption. The peak at around 802 cm^{-1} can be attributed to P–O bending in PO$_4^{3-}$ groups. The weak bands observed at around 1450 cm^{-1} are related to the presence of residual carbonate groups from the precursors
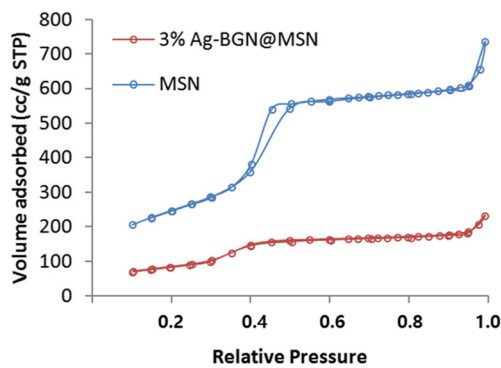
Fig. 3 Nitrogen adsorption-desorption isotherms of MSN and 3% Ag-BGN@MSN

plate-like particle. Table 1 shows the results of specific surface area (S_{BET}), pore volume (Vp), and pore diameter (Dp) using the BET and BJH methods. The pores in the MSNs measured 2.69 nm in diameter, whereas those in the Ag-BGN@MSN had a diameter of 2.51 nm. Similarly, their surface area/mass ratio differed drastically: 902.47 m^2/g in MSNs vs. 315.69 m^2/g in Ag-BGN@MSN. These results show that the pores of MSN were filled with Ag-BGN particles, and that the total pore volume was markedly greater in the Ag-BGN@MSN (3.62 cm^3/g) than in the MSNs (1.14 cm^3/g).

Field-emission scanning electron microscopy and field-emission transmission electron microscopy using energy-dispersive X-ray spectroscopy

The shape of the samples was observed using FESEM and 200 kV FETEM. The silica nanoparticle had a diameter of 100–350 nm on the FESEM image (Fig. 4a), while the BGN on the surface of MSN particle had a size of 30–50 nm (Fig. 4b). A more detailed image could be observed using 200 kV FETEM. Figure 5a shows the silica matrix surface of an MSN, and the Ag-BGN clusters coating the silica matrix can be seen in Fig. 5b. Through observation using 200 kV FETEM, it could be confirmed that the BGN coated the mesoporous structure of the compound.

Qualitative analysis of Ag$^+$ was performed using fast analytical energy-dispersive X-ray spectroscopy. Ag$^+$ was observed in the 1, 3, and 5% Ag-BGN@MSN (Fig. 6).

Table 1 N_2 adsorption results

Samples	SBET (m^2/g)	Vp (cc/g)	Dp (nm)
MSNs	902.47	1.14	2.69
Ag-BGN@MSN	315.69	3.62	2.51

S_{BET} (m^2/g) surface area, V_p (cc/g) total pore volume of pores with radius, D_p (nm) average pore radius

Field-emission scanning electron microscopy observation of tubule occlusion

Figure 7 shows the tubule-occluding effect in each group. Group 1 (Fig. 7(a1)–(d1)) depicts a dentin surface on which there is no smear layer due to the opening of dentinal tubule after soaking in 1 wt% citric acid solution for 20 s. Group 2 (Fig. 7(a2)–(d2)) and group 3 (Fig. 7(a3)–(d3)) show that both the BG and MSN particles penetrated and partly occluded the tubules. Group 4 (Fig. 7(a4)–(d4)) shows dentinal tubules that are completely occluded by compacted 3% Ag-BNG@MSN particles.

Fourteen days after soaking dentin disc in 6 wt% citric acid for 1 min, the amount of particles remaining on the dentin surface differed among the groups (Fig. 8). The diameter of the dentinal tubules had increased in group 1 (Fig. 8(a1)–(d1)). The amount of particles covering the tubule surface had decreased in group 2 (Fig. 8(a2)–(d2)) and group 3 (Fig. 8(a3)–(d3)). Furthermore, the depth of the MSN particle inside the remaining tubule had decreased in group 3 (Fig. 8(d3)). More tubule occlusion was observed in group 4 than in the other groups, and a membrane-like layer which completely covered the dentin surface had been observed in group 4 (Fig. 8(a4)–(d4)).

Occluding area ratio analysis

Table 2 shows the surface area ratio of the occluded dentinal tubules in each group before and after application of 6 wt% citric acid for 1 min. In the MSN and other groups, there was no significant difference in surface area ratio before and after the application of 6 wt% citric acid. However, the groups in which the BG and 3% Ag-BGN@MSNs were applied showed statistically significant differences ($P < 0.05$). After the application of 6 wt% citric acid, the ratio of occluded surface area decreased differently in each group. The greatest difference in this regard was observed in the BG group, while the MSN and 3% Ag-BGN@MSN groups showed little difference. It can be inferred that acid-resistant stability is higher in the MSN and 3% Ag-BGN@MSN groups.

MTBS test

Figure 9 and Table 3 show the mean and standard deviation of MTBS in each group. One-way ANOVA showed that there was no significant difference between the control group and the 3% Ag-BGN@MSN group ($P > 0.05$), but the Ag-BGN@MSN group did differ significantly from the BG and MSN groups ($P < 0.05$).

Cytotoxicity assay

Figure 10 shows the relative cell viability of the HDPCs exposed to 1, 3, and 5% Ag-BGN@MSN (0–320 μg/mL). The relative cell viability was more than 72% in all groups, and there were no

Fig. 4 Field-emission scanning electron microscopy images of the **a** MSNs and **b** 3% Ag-BGN@MSN
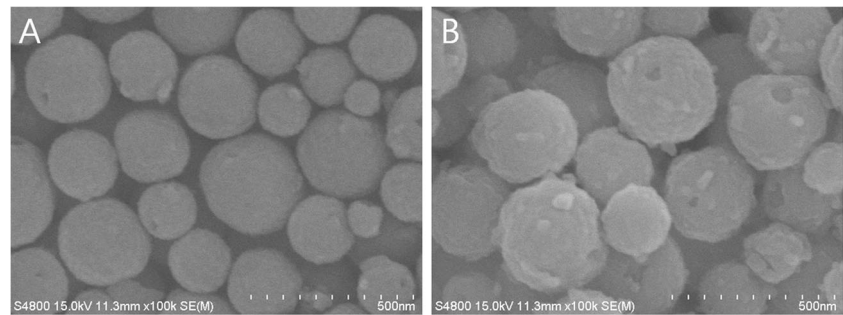
statistically significant differences in terms of sample density and time among HDPCS that had gone through 24-, 48-, and 72-h exposures (Fig. 10a–c). There were no significant differences among the pair-wise comparisons. ($P > 0.05$ in all cases).

Antibacterial effect test

Figure 11 shows the antibacterial properties of Ag-BGN@MSN. In the control group, *L. casei* incubated in MSNs had the highest light absorbance, indicating the most active bacterial growth. Light absorbance decreased as the density of 1, 3, and 5% Ag-BGN@MSN increased, and as the density of Ag^+ increased, suggesting that bacterial growth was inhibited.

In vitro ion dissolution test

Figure 12 shows the ion dissolution ability of Ag-BGN@MSN. Silver was not detected in the control group. In contrast, concentration of Ag^+ detected in the Ag-BGN@MSN group had rapidly increased to 6 ppm in 24 h. After 24 h, the time-dependent increment was not large, and the absolute concentration remained within 8.5 ppm. The concentration of Ca^{2+} was about 127 ppm in the control group; it rapidly increased to 300 ppm in the Ag-BGN@MSN group, showing little decrease or further increase thereafter. The concentration of PO_4^{3-} was 35.1 ppm in the control group; this rapidly dropped after 24 h to 2 ppm, and later to below 1.0 ppm.
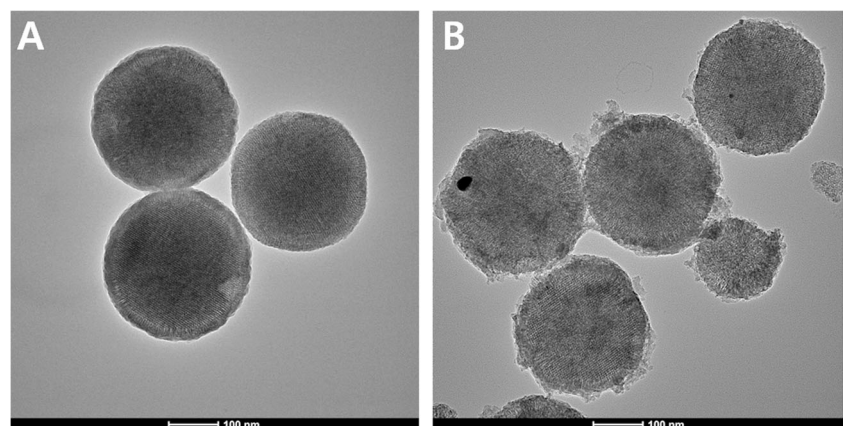
Discussion

From close examination of the synthesized Ag-BGN@MSN, it could be seen that the BG nanoparticle surrounded the MSN nanoparticle without invading its structure. This was because the MSN has excellent surface properties—a large surface area/mass ratio and pore volume, as well as a unique BGN-covering structure that is conferred during synthesis, because the MSN's high surface porosity acts as a nucleation site [29]. Furthermore, depending on the amount of silver added during synthesis, different densities of silver were observed on the surface of the MSN (Fig. 6). In the evaluation using N_2 adsorption-desorption isotherms, the surface area/mass ratio had decreased to 1/3 of its original size, although little decrease in pore radius was observed, even though the BGNs can affect the pore by forming a structure in the BGN that covers the MSN [30]. Conversely, the total pore volume of the Ag-BGN@MSNs had increased, perhaps because the volume between the BGNs formed through irregular bonding of the BGN particle to the surface of the MSN (Table 1).

Research into BG as a method of DH treatment has proceeded for long time [31, 32]. BGs induce remineralization on the dentin disc surface through ion dissolution and osteoconductivity [19], and hydroxycarbonate apatite precipitates created from this ion dissolution mechanically occlude the dentinal tubule [32]. However, BG particles themselves partially hinder the deposition of Ca^{2+} and PO_4^{3-}, thus delaying their effect [33]. In keeping with these previous observations, incomplete occlusion of the dentinal tubule was observed in the BG group of the present
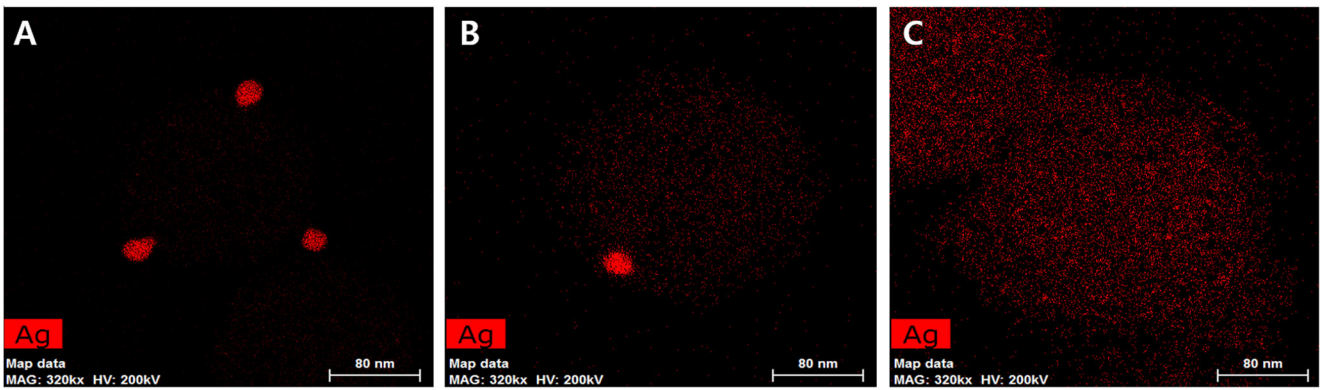
Fig. 5 200 kV field-emission transmission electron microscopy images of the **a** MSNs and **b** 3% Ag-BGN@MSN

Fig. 6 Fast analytical energy-dispersive X-ray spectroscopy of the **a** 1% Ag-BGN@MSN, **b** 3% Ag-BGN@MSN, and **c** 5% Ag-BGN@MSN

study (Fig. 7(a2)–(d2)). The MSN is a spherical particle with a diameter of 100–350 nm; it showed deeper dentinal tubule occlusion (3–4 μm) than the other materials. However, since the MSN penetrated the dentinal tubule in the form of a particle,

compact occlusion of the dentinal tubule to the wall did not occur (Fig. 7(a3)–(d3)). The Ag-BGN@MSN showed more complete wall occlusion than the other materials (Fig. 7(a4)–(d4)), with the BGNs effectively filling the empty space among the MSN
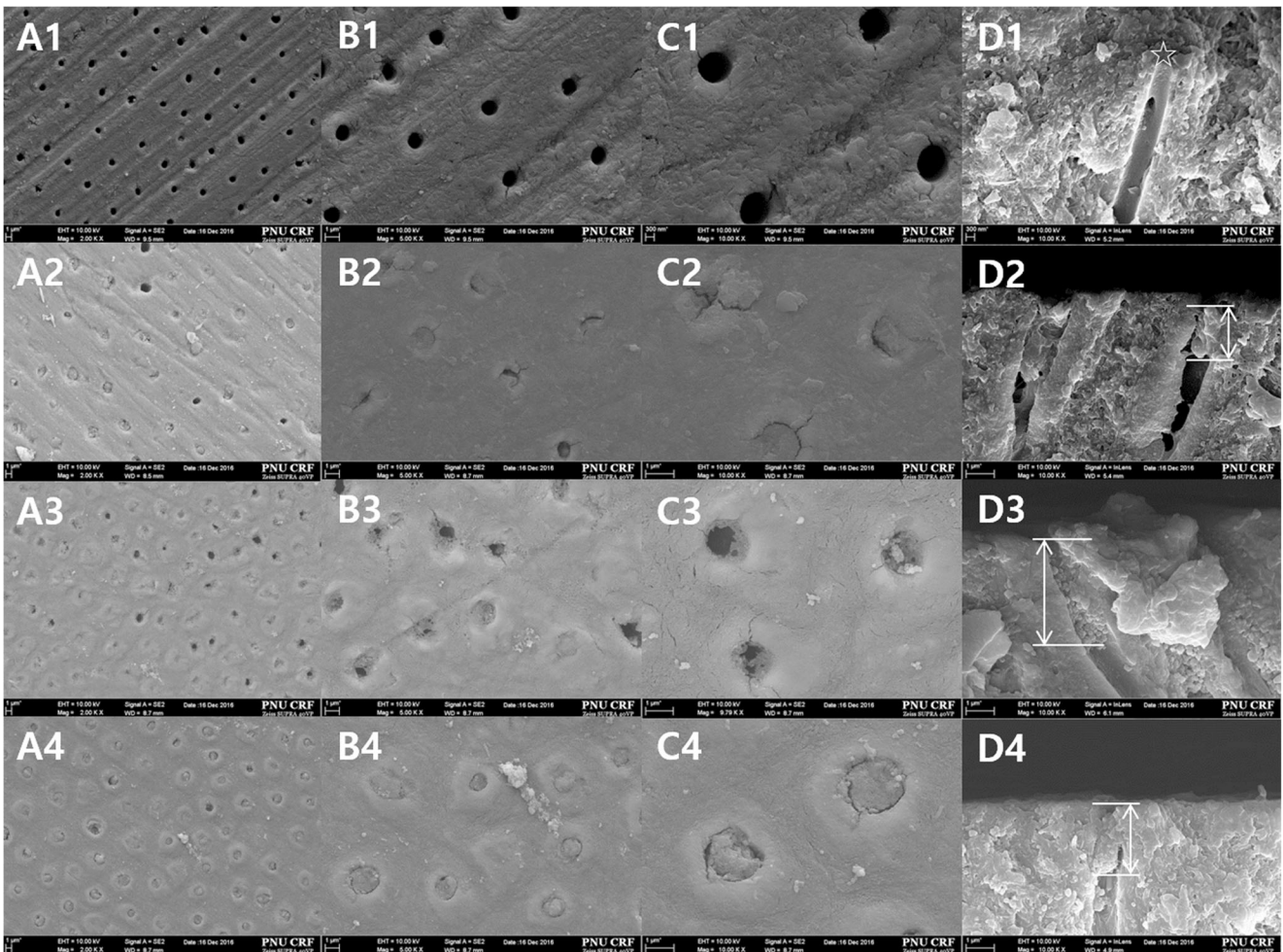

Fig. 7 Field-emission scanning electron microscopy micrographs (A: ×2000, B: ×5000, C: ×10,000) of the superior and axial surfaces to evaluate the tubule-occluding effect in each group. No smear layer was observed in the dentinal tubules on the images of group 1 (control; a1–d1). *The image from group 2 (BG) shows dentinal tubules that are

partially occluded to a depth of 1–2 μm (arrow). On the image from group 3 (MSN), the dentinal tubules are partially occluded to a depth of 3–4 μm, and the particles were scattered. Group 4 (3% Ag-BNG@MSN) shows dentinal tubules that are completely occluded by particles to a depth of 2–3 μm (arrow)
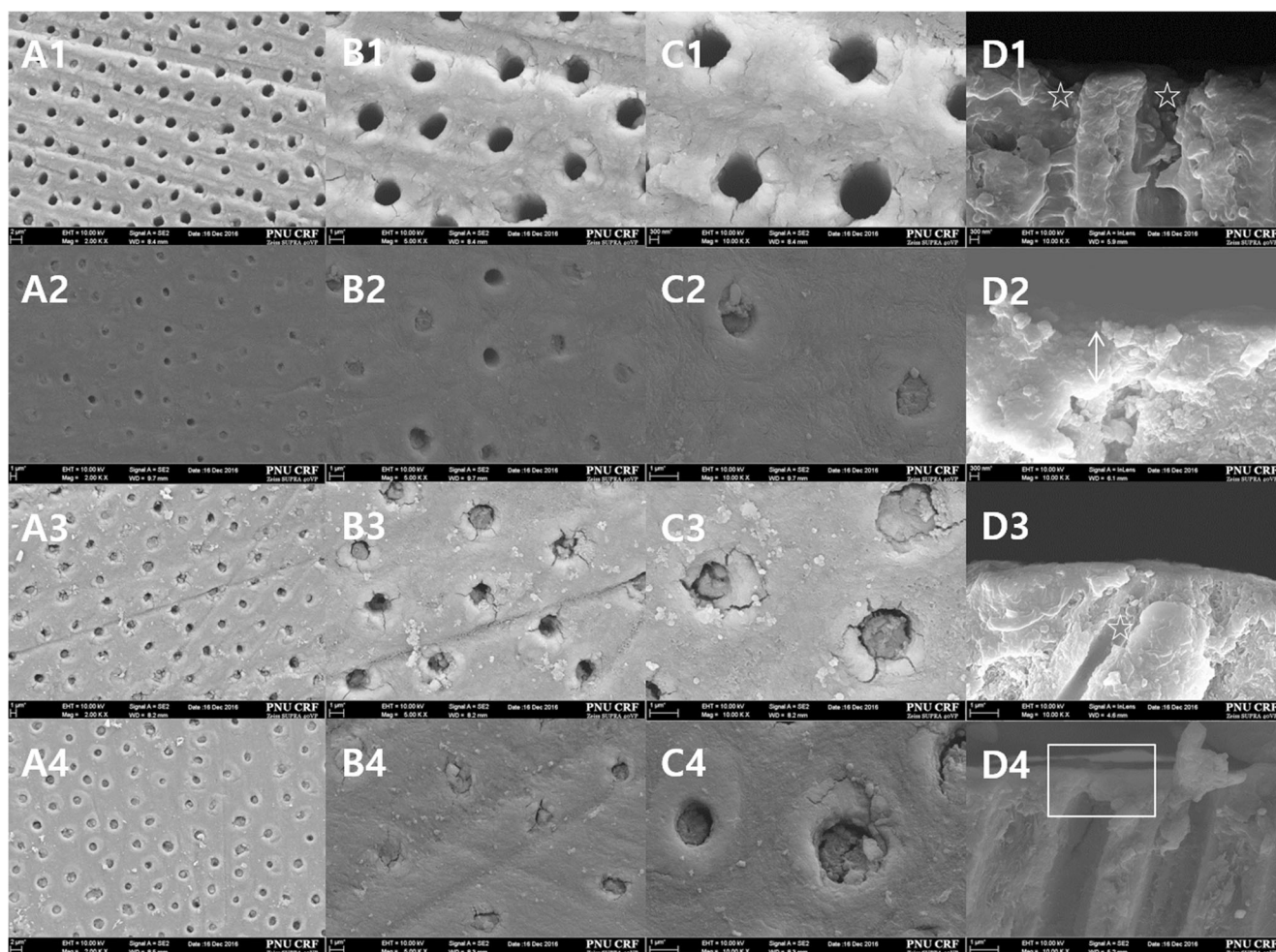
Fig. 8 Field-emission scanning electron microscopy micrographs (A: ×2000, B: ×5000, C: ×10,000) of the superior and axial surface to evaluate the tubule-occluding effect in each group 14 days after exposure to 6 wt% citric acid solution for 1 min. Images of group 1 (control; a1–d1) show an increase in the diameter of the dentinal tubule (star). The images of group 2 (BG) show a decrease in the number of particles occluding the dentinal tubules. The image of group 3 (MSN) indicates that the depth of particle inside of tubule, as well as the number of particles occluding the dentinal tubule, had decreased. In the image of group 4 (3% Ag-BNG@MSN), a membrane-like layer (box) covering the dentin surface can be seen. Most of the dentinal tubules were occluded in group 4

particles. Secondarily, dentinal tubule sealing through the formation of a hydroxycarbonate apatite layer from the BG accelerates complete occlusion of the tubule.

Acid-resistant stability is a key factor in the long-term prognosis of DH treatment. Citric acid is a very common substance in the diet; therefore, 6 wt% citric acid was used to simulate the intraoral environment in the present experiment [14]. In addition,

careful attention must be paid to citric acid, because it can dissolve calcium phosphate [34]. The acid-resistant stability was assessed by observing structural changes in the dentinal tubules. The size of the dentinal tubule had increased after soaking dentin disc in a 6 wt% citric acid, as expected (Fig. 8(a1)–(d1)). This was because, in acidic conditions, the degree of mineralization of peritubular dentin is larger than that of intertubular dentin [14].
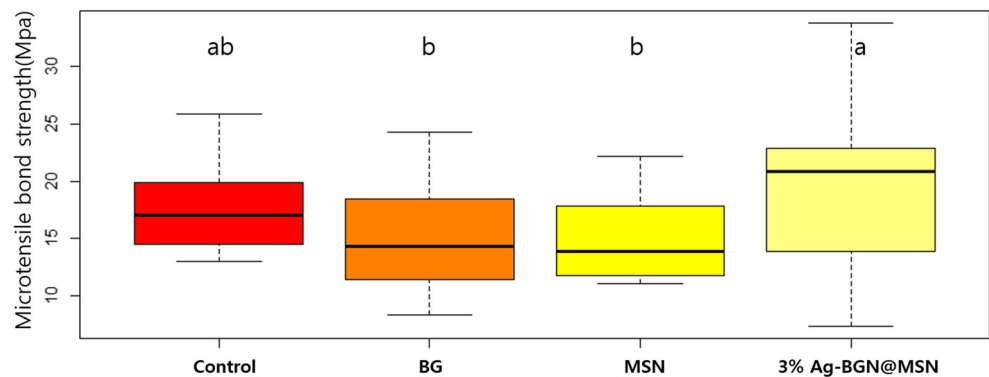
Table 2 Surface area ratio of the occluded dentinal tubule

Groups	Occluded area (%)	
	Before acid challenge*	After acid challenge*
BG	74.46 ± 12.74^{b}	49.12 ± 14.77^{c}
MSN	78.89 ± 5.12^{ab}	71.62 ± 15.65^{b}
3% Ag-BGN@MSN	93.14 ± 4.88^{a}	83.04 ± 7.51^{ab}

The same superscript was used for all means that were not significantly different ($P < 0.05$)

*ANOVA was performed

Fig. 9 Microtensile bond strength in the control, BG, MSN, and 3% Ag-BGN@MSN groups *ANOVA was performed. The same superscript is used for all means that are not significantly different ($P < 0.05$)

After acid exposure, most of the dentinal surface BG was removed, and the remaining BG was superficially occluding the tubule entrance (Fig. 8(a2)–(d2)). In addition, the area ratio of the occluded dentinal tubule had decreased by about 25% (Table 2). As has been reported previously, the dentinal tubule's sealing effect decreased when the BG was exposed to acidic conditions, confirming that the tubule was reopened as the calcium phosphate deposits inside the dentinal tubule were dissolved.

In the MSN-treatment group, the area ratio of dentinal tubule occlusion was similar to that in BG group. However, after acidic exposure, there was a roughly 7% decrease in the area of the occluded dentinal tubule, indicating that the MSNs had higher acid-resistant stability than the BGs ($P < 0.05$; Table 2). This phenomenon is likely due to unique acid resistance of mesoporous silica. However, in the MSN-treatment group, there was a considerable amount of space among the MSNs before acidic exposure; therefore, the MSNs were washed off by the citric acid, resulting in a decreased depth of dentinal tubule occlusion (Fig. 8(d3)).

The Ag-BGN@MSN-treatment group had the highest rate of dentinal tubule occlusion of all the groups ($P < 0.05$). Furthermore, the Ag-BGN@MSN-treatment group had a higher rate of dentinal tubule reopening after acidic exposure than the MSN group. Nonetheless, the group still showed highest total ratio of dentinal tubule occlusion (Table 2). In addition, a membrane-like layer could be observed on the dentin surface

(Fig. 8(d4)). It follows that the Ag-BGN@MSN group had the highest acid-resistant stability.

Moreover, the tubule-occluding ability of MSNs was also enhanced by adding BGNs, which has high acid-resistant stability, allowing it to fill the empty spaces among the MSN particles. This enhanced tubule-occluding ability and apatite formation inside dentinal tubule likely contributed to the increase in acid-resistant stability.

According to recent research, the silanol group on the MSN surface creates an active, nano-sized, carbonated apatite [29], and 50 nm silica nanoparticles inhibit osteoclast differentiation and induce osteoblast differentiation, so that bone mineral density increases. However, in the present study, no membrane-like layer formed in the MSN-treatment group, as was evident from the observation that pure mesoporous silica materials (MCM-41) did not present bioactive behavior [35]. Conversely, phosphorous- or BG-doped mesoporous silica materials induce the formation of an apatite layer [30, 37]. Like the MCM-41, MSNs cannot create an apatite layer because it has small pore size and volume. On the other hand, in the Ag-BGN@MSN group, a membrane-like layer was likely formed, because Ag-BGN@MSNs have large pore volume. Additionally, BG dilutes ions such as calcium, phosphate, silanol, and sodium to induce remineralization, a process that becomes faster as the BG becomes smaller [36]. Thus, MSNs doped with 30–50 nm BGN probably formed a membrane-like layer in the present study. In conclusion, because more dentinal tubules were occluded by Ag-BGN@MSN, there was better tubular wall occlusion in this group. Moreover, because a membrane-like layer formed, the acid-resistant stability likely increased. Thus, dentinal tubule sealing induced by Ag-BGN@MSN is likely to increase long-term stability in DH treatment.

In a clinical environment, resin restoration follows treatment for DH. For this reason, dentists must investigate how the DH treatment agent affects the MTBS between dentin and adhesive. Theoretically, the DH treatment methods that accompany dentinal tubule occlusion reduce the bonding strength, because such methods make it hard for the resin tag to form, thus interrupting the mechanical locking of the resin [38]. However, our experimental results showed that

Table 3 Microtensile bond strength

Sample	Mean (Mpa)
Control	17.61 ± 3.63[ab]
BG	14.99 ± 4.76[b]
MSN	15.16 ± 3.65[b]
3% Ag-BGN@MSN	19.57 ± 7.44[a]

ANOVA was performed. The same superscript was used for all means that were not significantly different ($P < 0.05$)

BG bioactive glass, *MSN* mesoporous silica nanoparticle, *Ag-BGN@MSN* silver-doped bioactive glass coated mesoporous silica nanocomposite
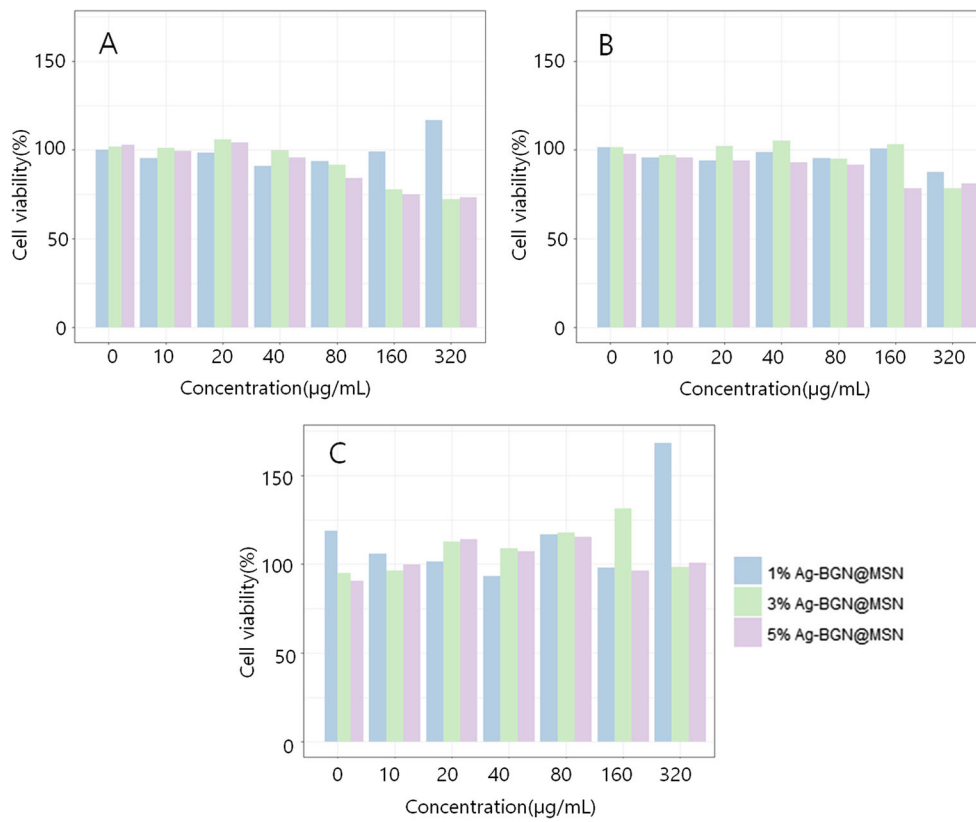
Fig. 10 Relative cell viability of human dental pulp cells exposed to different densities (0–320 μg/mL) of 1%, 3%, and 5% Ag-BGN@MSN for 24 (**a**), 48 (**b**), and 72 h (**c**)

there were no significant differences between any of the three groups and the control group ($P > 0.05$). This was likely due to the following factors: 10-methacryloyloxydecyl dihydrogen phosphate, the monomer of the Clearfil SE Bond, in addition to its mechanical locking, reacts and bonds with free calcium

to provide extra bonding force between resin and dentin [39]. Similarly, the BG, MSN, and Ag-BGN@MSN solutions increase surface wettability and reduce surface tension. High surface wettability and low surface tension contribute to a low contact angle and high surface energy, which generally

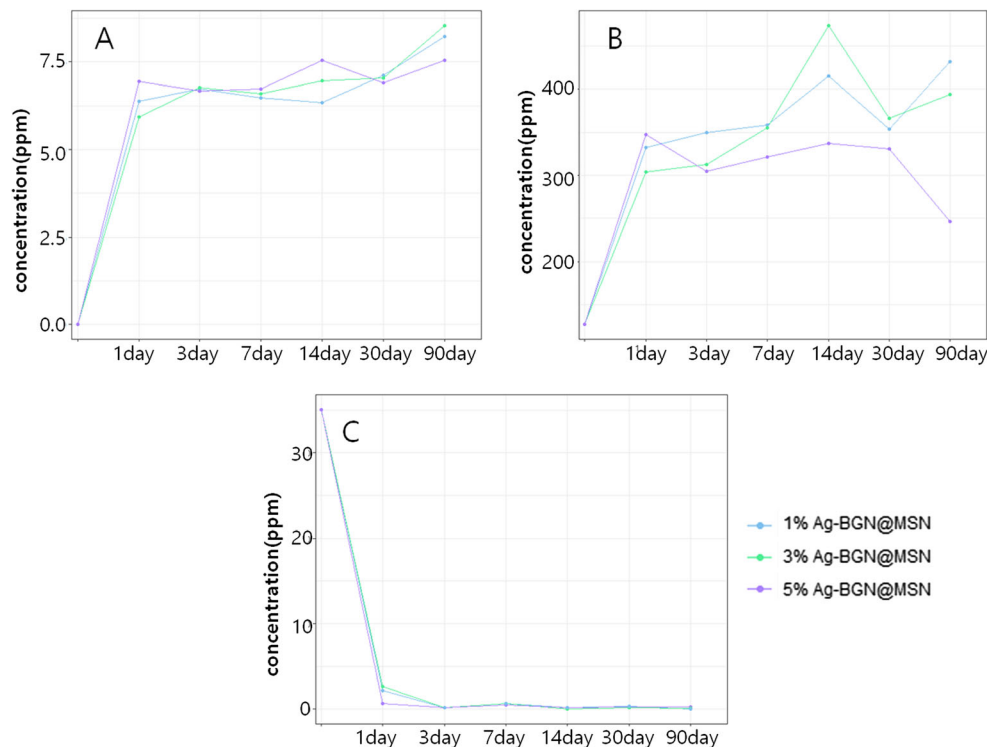**Fig. 11** Antibacterial properties of MSNs and 1, 3, and 5% Ag-BGN@MSN (0–1000 μg/mL; 24 h)
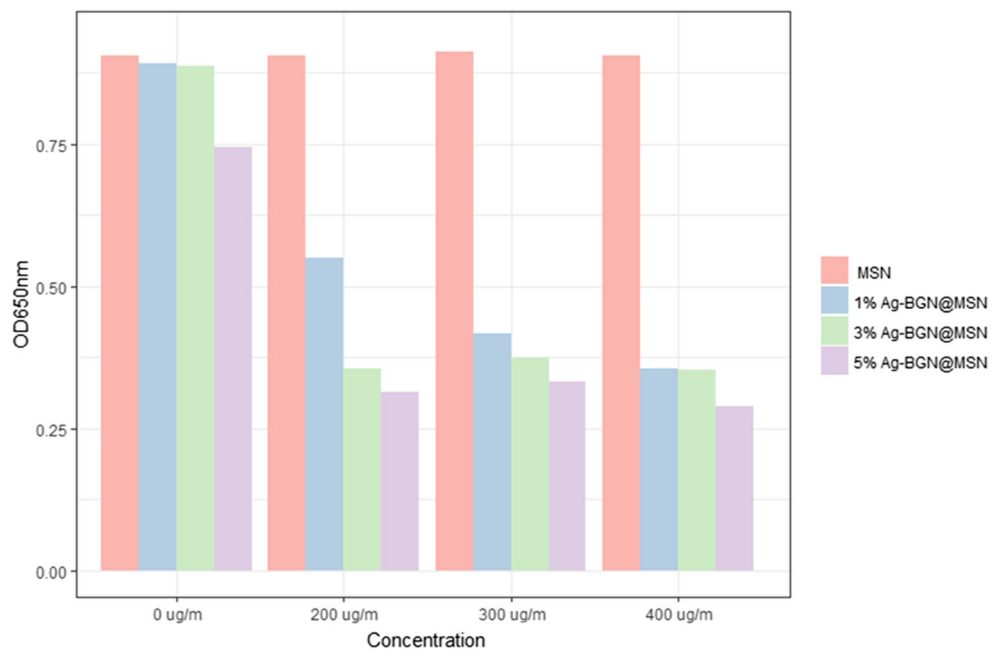
Fig. 12 Changes in **a** Ag$^+$ concentration over time, **b** calcium concentration over time, and **c** phosphate concentration over time

help mechanical locking and adhesion [40]. Furthermore, weak sections of the hybrid layer would be complemented by precipitates below the dentin collagen [41]. For the same reasons, bonding strength probably does not decrease after the treatment agent is applied.

Ag-BGN@MSN must have low cytotoxicity to be used clinically. For this reason, in vitro cytotoxicity was evaluated using the MTT assay. When 0–320 μg/mL density of 1, 3, and 5% Ag-BGN@MSN was applied to HDPCs for 24, 48, and 72 h, all the Ag-BGN@MSNs had a relative cell viability above 72% (Fig. 10). Thus, Ag-BGN@MSN is likely to be biocompatible, and it can therefore be used in vivo.

To evaluate the antibacterial ability of the silver ions added during synthesis, *L. casei* was used. *L. casei*, usually produces lactic acid during glucose fermentation; it can readily be found on deep caries lesions, and is rarely found before caries development or during early tooth decay. In particular, it acts as a pioneering microorganism when caries progress into the dentin [42]. When *L. casei* was incubated in 0–400 μg/mL density of 1, 3, 5% Ag-BGN@MSN, bacterial growth was inhibited by more than 50% (Fig. 11). It follows that Ag-BGN@MSN has an antibacterial effect against *L. casei*.

Finally, to evaluate in vitro changes in ion density that depend on bioactivity, stimulated body fluid was used, which has a similar composition and ion density to that of human plasma. Remineralization and antibacterial ability was estimated by measuring the density of Ca^{2+} and PO$_4^{3-}$ ions required for remineralizaition, as well as that of

Ag$^+$—an ion related to antibacterial ability. In 1, 3, and 5% Ag-BGN@MSN, the Ag$^+$ density had increased rapidly to about 6 ppm within 24 h, and it remained at this level afterwards. Based on previous studies, which have stated that when any Ag$^+$ density higher than 0.05 ppm presents an antibacterial effect against *Staphylococcus aureus* and *Escherichia coli* [43], it can be assumed that 1, 3, and 5% Ag-BGN@MSN all have an antibacterial effect. The density of Ca^{2+} rapidly increased to about 300 ppm within 24 h, and it either decreased or increased subsequently. This occurred because the Ca^{2+} balance resulted from the vitreous component of the Ag-BGN@MSN [2]. Since the vitreous component releases cations into the media, an increase in Ca^{2+} density is observed, and as an apatite layer is later formed, the density of Ca^{2+} is partly decreased. The density of phosphate rapidly dropped as time passed, probably because of phosphate crystallization [44].

To summarize, the Ag-BGN@MSN biocomposite is capable of successful occlusion of dentin tubules; in addition, it has acid-resistance stability. Because Ag-BGN@MSN does not affect bonding strength, it has little cytotoxicity, and it presents an antibacterial effect. Therefore, it is considered to be effective in the treatment of DH.

However, the intraoral environment is different from an experimental set up, so further in vivo study is required. Moreover, further assessment of the antibacterial ability of silver against other harmful bacterium besides *L. casei* may be needed.

Conclusion

In the present study, BG and MSN were used as substances that present a treatment effect by effectively occluding the dentinal tubule. It can be confirmed that an Ag-BGN@MSN biocomposite, which was synthesized using an applied version of the BG synthesis method (the sol-gel method), was successfully processed using XRD, FT-IR, FESEM, FETEM, and BET. For the treatment of DH, Ag-BGN@MSN successfully occluded the exposed dentin tubule; it also presented acid-resistant stability. Finally, it did not hinder the MTBS between dentin and the adhesive system, did not have cytotoxicity in the in vitro experiment, and presented an antibacterial effect. Thus, it can be confirmed that the Ag-BGN@MSN biocomposite compound is an effective material for the treatment of DH.

Compliance with ethical standards

Conflict of interest YI Kim has received research grants from the National Research Foundation of Korea (NRF) for this study. All authors declare that they have no competing interest.

Ethical approval The study was approved by the Ethics Committee of Pusan National University Dental Hospital (PNUDH-2016-033).

Informed consent Informed consent was obtained from all individual participants included in the study.

Reference

1. Sanjay M, Vivek A, Bhoomika A (2010) Dentin hypersensitivity: recent trends in management. J Conserv Dent 13:218–224. https://doi.org/10.4103/0972-0707.73385
2. Holland GR, Narhi MN, Addy M, Gangarosa L, Orchardson R (1997) Guidelines for the design and conduct of clinical trials on dentine hypersensitivity. J Clin Periodontol 24:808–813. https://doi.org/10.1111/j.1600-051X.1997.tb01194.x
3. Brannstrom M (1963) Dentin sensitivity and aspiration of odontoblasts. J Am Dent Assoc 66:366–370. https://doi.org/10.14219/jada.archive.1963.0104
4. Rees JS, Jin U, Lam S, Kudanowska I, Vowles R (2003) The prevalence of dentine hypersensitivity in a hospital clinic population in Hong Kong. J Dent 31:453–461. https://doi.org/10.1016/S0300-5712(03)00092-7
5. Flynn J, Galloway R, Orchardson R (1985) The incidence of 'hypersensitive' teeth in the West of Scotland. J Dent 13:230–236. https://doi.org/10.1016/0300-5712(85)90004-1
6. Fischer C, Fischer RG, Wennberg A (1992) Prevalence and distribution of cervical dentine hypersensitivity in a population in Rio de Janeiro, Brazil. J Dent 20:272–276. https://doi.org/10.1016/0300-5712(92)90043-C
7. Wang Y, Que K, Lin L, Hu D, Li X (2012) Prevalence of dentine hypersensitivity in the general population in China. J Oral Rehabil 39:812–820. https://doi.org/10.1111/j.1365-2842.2012.02334.x
8. Liu HC, Lan WH, Hsieh CC (1998) Prevalence and distribution of cervical dentin hypersensitivity in a population in Taipei, Taiwan. J Endod 24:45–47. https://doi.org/10.1016/S0099-2399(98)80213-6
9. Absi EG, Addy M, Adams D (1987) Dentine hypersensitivity: a study of the patency of dentinal tubules in sensitive and non-sensitive cervical dentine. J Clin Periodontol 14:280–284. https://doi.org/10.1111/j.1600-051X.1987.tb01533.x
10. Schmidlin PR, Sahrmann P (2013) Current management of dentin hypersensitivity. Clin Oral Investig 17:55–59. https://doi.org/10.1007/s00784-012-0912-0
11. Pashley DH (1994) Dentin permeability and its role in the pathobiology of dentin sensitivity. Arch Oral Biol 39:73–80. https://doi.org/10.1016/0003-9969(94)90191-0
12. Wang Z, Sa Y, Sauro S, Chen H, Xing W, Ma X (2010) Effect of desensitising toothpastes on dentinal tubule occlusion: a dentine permeability measurement and SEM in vitro study. J Dent 38:400–410. https://doi.org/10.1016/j.jdent.2010.01.007
13. Canali GD, Rached RN, Mazur RF, Souza EM (2017) Effect of erosion/abrasion challenge on the dentin tubule occlusion using different desensitizing agents. Braz Dent J 28:216–224. https://doi.org/10.1590/0103-6440201700811
14. Reis C, De-Deus G, Leal F, Azevedo E, Coutinho-Filho T, Paciornik S (2008) Strong effect on dentin after the use of high concentrations of citric acid: an assessment with co-site optical microscopy and ESEM. Dent Mater 24:1608–1615. https://doi.org/10.1016/j.dental.2008.03.027
15. Wiegand A, Stock A, Attin R, Werner C, Attin T (2007) Impact of the acid flow rate on dentin erosion. J Dent 35:21–27. https://doi.org/10.1016/j.jdent.2006.04.002
16. Pei D, Liu S, Huang C, Du X, Yang H, Wang WY (2013) Effect of pretreatment with calcium-containing desensitizer on the dentine bonding of mild self-etch adhesives. Eur J Oral Sci 121:204–210. https://doi.org/10.1111/eos.12047
17. Tang F, Li L, Chen D (2012) Mesoporous silica nanoparticles: synthesis, biocompatibility and drug delivery. Adv Mater 24:1504–1534. https://doi.org/10.1002/adma.201104763
18. Huang X, Young NP, Townley HE (2014) Characterisation and comparison of mesoporous silica particles for optimised drug delivery. Nanomater Nanotechnol 4:2–15. https://doi.org/10.5772/58290
19. Tian L, Peng C, Shi Y, Guo X, Zhong B, Qi J et al (2014) Effect of mesoporous silica nanoparticles on dentinal tubule occlusion: an in vitro study using SEM and image analysis. Dent Mater J 33:125–132. https://doi.org/10.4012/dmj.2013-215
20. Prabhakar AR, Paul MJ, Basappa N (2010) Comparative evaluation of the remineralizing effects and surface micro hardness of glass ionomer cements containing bioactive glass (S53P4): an in vitro study. Int J Clin Pediatr Dent 3:69–77. https://doi.org/10.5005/jp-journals-10005-1057
21. Erol-Taygun M, Zheng K, Boccaccini AR (2013) Nanoscale bioactive glasses in medical applications. Int J Appl Glas Sci 4:136–148. https://doi.org/10.1111/ijag.12029
22. Webster TJ, Ergun C, Doremus RH, Siegel RW, Bizios R (2000) Enhanced functions of osteoblasts on nanophase ceramics. Biomaterials 21:1803–1810. https://doi.org/10.1016/S0142-9612(00)00075-2
23. Miguez-Pacheco V, Hench LL, Boccaccini AR (2015) Bioactive glasses beyond bone and teeth: emerging applications in contact with soft tissues. Acta Biomater 13:1–15. https://doi.org/10.1016/j.actbio.2014.11.004
24. Hoppe A, Güldal NS, Boccaccini AR (2011) A review of the biological response to ionic dissolution products from bioactive glasses

and glass-ceramics. Biomaterials 32:2757–2774. https://doi.org/10.1016/j.biomaterials.2011.01.004

25. Ruparelia JP, Chatterjee AK, Duttagupta SP, Mukherji S (2008) Strain specificity in antimicrobial activity of silver and copper nano-particles. Acta Biomater 4:707–716. https://doi.org/10.1016/j.actbio.2007.11.006

26. El-Kady AM, Ali AF, Rizk RA, Ahmed MM (2012) Synthesis, characterization and microbiological response of silver-doped bio-active glass nanoparticles. Ceram Int 38:177–188. https://doi.org/10.1016/j.ceramint.2011.05.158

27. Shi X, Wang Y, Wei K, Ren L, Lai C (2008) Self-assembly of nanohydroxyapatite in mesoporous silica. J Mater Sci Mater Med 19:2933–2940. https://doi.org/10.1007/s10856-008-3424-3

28. Xia W, Chang J (2007) Preparation and characterization of nano-bioactive-glasses (NBG) by a quick alkali-mediated sol–gel meth-od. Mater Lett 61:3251–3253. https://doi.org/10.1016/j.matlet.2006.11.048

29. Wang Y, Zhao Q, Han N, Bai L, Li J, Liu J, Che E, Hu L, Zhang Q, Jiang T, Wang S (2015) Mesoporous silica nanoparticles in drug delivery and biomedical applications. Nanomedicine 11:313–327. https://doi.org/10.1016/j.nano.2014.09.014

30. Horcajada P, Rámila A, Boulahya K, González-Calbet J, Vallet-Regí M (2004) Bioactivity in ordered mesoporous materials. Solid State Sci 6:1295–1300. https://doi.org/10.1016/j.solidstatesciences.2004.07.026

31. Lee BS, Chang CW, Chen WP, Lan WH, Lin CP (2005) In vitro study of dentin hypersensitivity treated by Nd:YAP laser and bioglass. Dent Mater 21:511–519. https://doi.org/10.1016/j.dental.2004.08.002

32. Chiang YC, Chen HJ, Liu HC, Kang SH, Lee BS, Lin FH (2010) A novel mesoporous biomaterial for treating dentin hypersensitivity. J Dent Res 89:236–240. https://doi.org/10.1177/0022034509357148

33. Yu J, Yang H, Li K, Lei J, Zhou L, Huang C (2016) A novel application of nanohydroxyapatite/mesoporous silica biocomposite on treating dentin hypersensitivity: an in vitro study. J Dent 50:21–29. https://doi.org/10.1016/j.jdent.2016.04.005

34. Xu Z, Neoh KG, Kishen A (2008) Monitoring acid-demineralization of human dentine by electrochemical impedance spectroscopy (EIS). J Dent 36(12):1005–1012. https://doi.org/10.1016/j.jdent.2008.08.007

35. Izquierdo-Barba I, Ruiz-González L, Doadrio JC, González-Calbet JM, Vallet-Regí M (2005) Tissue regeneration: a new property of mesoporous materials. Solid State Sci 7:983–989. https://doi.org/10.1016/j.solidstatesciences.2005.04.003

36. Vollenweider M, Brunner TJ, Knecht S, Grass RN, Zehnder M, Imfeld T, Stark WJ (2007) Remineralization of human dentin using ultrafine bioactive glass particles. Acta Biomater 3:936–943. https://doi.org/10.1016/j.actbio.2007.04.003

37. Vallet-Regí M, Izquierdo-Barba I, Rámila A, Pérez-Pariente J, Babonneau F, González-Calbet JM (2005) Phosphorous-doped MCM-41 as bioactive material. Solid State Sci 7:233–237. https://doi.org/10.1016/j.solidstatesciences.2004.10.038

38. Adebayo OA, Burrow MF, Tyas MJ (2008) Dentine bonding after CPP-ACP paste treatment with and without conditioning. J Dent 36:1013–1024. https://doi.org/10.1016/j.jdent.2008.08.011

39. Bergamin AC, Bridi EC, Amaral FL, Turssi CP, Basting RT, Aguiar FH, França FM (2016) Influence of an arginine-containing tooth-paste on bond strength of different adhesive systems to eroded dentin. Gen Dent 64:67–73

40. Marshall SJ, Bayne SC, Baier R, Tomsia AP, Marshall GW (2010) A review of adhesion science. Dent Mater 26:11–16. https://doi.org/10.1016/j.dental.2009.11.157

41. Yang H, Pei D, Liu S, Wang Y, Zhou L, Deng D (2013) Effect of a functional desensitizing paste containing 8% arginine and calcium carbonate on the microtensile bond strength of etch-and-rinse ad-hesives to human dentin. Am J Dent 26:137–142. https://doi.org/10.1186/s40563-014-0024-y

42. Karpiński TM, Szkaradkiewicz AK (2013) Microbiology of dental caries. J Biol Earth Sci 3:21–24. https://doi.org/10.1007/978-1-349-16547-6_3

43. Jung WK, Koo HC, Kim KW, Shin S, Kim SH, Park YH (2008) Antibacterial activity and mechanism of action of the silver ion in *Staphylococcus aureus* and *Escherichia coli*. Appl Environ Microbiol 74:2171–2178. https://doi.org/10.1128/AEM.02001-07

44. Brown ML, Davis HB, Tufekci E, Crowe JJ, Covelle DA, Mitchell JC (2011) Ion release from a novel orthodontic resin bonding agent for the reduction and/or prevention of white spot lesions: an in vitro study. Angle Orthod 81:1014–1020. https://doi.org/10.2319/120710-708.1